



OPEN

# Enhanced trion emission from colloidal quantum dots with photonic crystals by two-photon excitation

SUBJECT AREAS:

TWO-DIMENSIONAL  
MATERIALS

QUANTUM DOTS

Xingsheng Xu

Received  
17 September 2013Accepted  
30 October 2013Published  
15 November 2013Correspondence and  
requests for materials  
should be addressed to  
X.S.X. (xsxu@semi.ac.  
cn)

State Key Laboratory of Integrated Optoelectronics, Institute of Semiconductors, Chinese Academy of Sciences, Beijing 100083, China.

For colloidal quantum dots, the ongoing biggest problem is their fluorescence blinking. Until now, there is no generally accepted model for this fluorescence blinking. Here, two-photon excited fluorescence from CdSe/ZnS nanocrystals on silicon nitride photonic crystals is studied using a femtosecond laser. From analysis of the spectra and decay processes, most of the relative trion efficiency is larger than 10%, and the largest relative trion efficiency reaches 46.7%. The photonic crystals enhance the trion emission of CdSe/ZnS nanocrystals, where the enhancement is due to the coupling of the trion emission to the leaky mode of the photonic crystal slab. Moreover, the photonic crystals enhance the Auger-assisted trapping efficiency of electrons/holes to surface states, and then enhance the efficiency of the generations of charge separation and DC electric field, which modifies the trion spectrum. Therefore, a model is present for explaining the mechanism of fluorescence blinking including the effect of the environment.

Fluorescence intermittency is one of the few remaining challenging problems in quantum mechanisms, and it is a significant weakness for applications in quantum information. Photoluminescence (PL) intermittency is mainly interpreted as being caused by charging and discharging of nanocrystals<sup>1</sup>, where charged quantum dots (QDs) are weak emitters due to fast nonradiative Auger recombination of excitons. However, some other models that are supported by experimental results and theoretical analysis indicate that fluorescence intermittency may be triggered by random activation of nonradiative exciton traps at the surface of nanocrystals<sup>2</sup>. Researchers measured the lifetime of negatively charged cores as being of the order of tens of microseconds in nanocrystal films, and it was found that nanocrystal photoionization occurs through Auger processes<sup>3</sup>. Measurement of PL decay has provided directly the lifetime of trion emission. It was found that the lifetime of a trion is indeed longer than that of a bi-exciton and also that its radiative rate is faster than the exciton radiative rate at room temperature. The results imply a 10–15% quantum yield for trions that may be too bright for the *off* state seen in blinking<sup>4</sup>. An intermediate state was observed in the blinking of single CdSe/CdS core-shell nanocrystals. This state has a low quantum yield higher than the “*off*” state and much lower than the “*on*” state observed in the PL blinking of individual nanocrystals. The observed values of those states are consistent with photoinduced, adsorption/desorption events that take place at the surface of the nanocrystals<sup>5</sup>. The surface state results in the dim state facilitating the transition to the *off* state and an increase of nonradiative relaxation due to the formation of trion emission.

Controlling spontaneous emission from QDs by PhCs is attractive and useful. The effective control of spontaneous emission by photonic crystals (PhCs) has been extensively studied<sup>6–8</sup>. Spontaneous emission from QDs is strongly modified as the photonic band gap covers the QD emission wavelength range<sup>9</sup>. Interaction between high-Q PhC nanocavity and spontaneous emission from QDs has been exploited<sup>10,11</sup>. Modification of spectra was found, as well as extraction of spontaneous emission from PhCs<sup>12,13</sup>. PhC patterns can enhance the external quantum efficiency of spontaneous emission<sup>13–19</sup>. Most of the literature cited above is related to linearly excited fluorescence, and there are few reports on two-photon excited fluorescence (TPF) controlled by PhCs<sup>20</sup>. Here, the significant modification of spectra for TPF is observed and analysed, and a blue shift of the spectrum of TPF from CdSe QDs on SiN PhCs is found. This blue shift is attributed to positive trion<sup>3–5</sup> emission and the coupling of the emission into the leaky mode of the PhC slab<sup>20</sup>. This is the first report of the enhancement of charged exciton (trion) emission by two-dimensional PhCs. Both the spectrum and the decay process of QDs on PhCs directly demonstrate that the relative trion efficiency is higher than 10%, which is too bright for the *off* state observed in the blinking phenomenon. It has been proved that for an emitter with emission located at the photonic band, the



radiative rate changes less than 20%<sup>21</sup>. PhCs provide us with a new tool to explore the photo-physics mechanism for fluorescence blinking of single emitters.

## Results

**TPF spectra from QDs on PhCs.** Amorphous silicon nitride (SiN) PhCs and CdSe QDs were prepared as described elsewhere<sup>22</sup>. A fabricated PhC is shown in Fig. S1. We measured the spectra of TPF from CdSe/ZnS QDs on PhCs with different lattice constants (see methods). The spectra of QDs on PhCs are fitted to a Gaussian function; some fitting curves and corresponding original experimental data are shown in Fig. S2. The coincidence between the experimental data and the Gaussian function differs for the different lattice constants. For lattice constants of 1250 nm and 700 nm (representing a significant blue shift), both the right- and left-hand sides of the spectra cannot be fitted well to the Gaussian function. For the lattice constant of 950 nm, the right-hand side of the spectrum fits relatively well to the Gaussian function, but on the left-hand side, there is a weak spectral peak, which is more distinct for the spectrum for the lattice constant of 1250 nm. The coincidence for the fitting of the spectra for lattice constants of 700 nm or 650 nm is worse, although their PL intensities are much lower than that for the lattice constant of 1250 nm. The spectra for lattice constants of 1500 nm or 900 nm can be fitted fairly well to the Gaussian function, and there is no obvious peak on the short-wavelength side.

The normalized spectra from the QDs on PhCs and those on blank SiN material are compared in Fig. 1, which shows normalized spectra for PhC lattice constants of 1250 nm, 1000 nm, 800 nm, 750 nm, 700 nm and 600 nm, and the spectrum from QDs without PhC. The profiles of the spectra are different for PhCs with different lattice constants. Compared with the spectra from QDs on blank SiN without PhCs, the spectra from QDs on PhCs undergo a blue shift, and the shift values vary with the PhC lattice constant. The average centre wavelength of the spectrum from QDs on blank without PhC is 586.38 nm. For a lattice constant of 1250 nm, the central wavelength of the spectrum from this PhC is 582.50 nm by fitting with a Gaussian function, and the blue shift is 3.9 nm compared with the blank. For lattice constants of 1000 nm and 800 nm, the central peak wavelengths are 581.12 nm and 575.79 nm, and the blue shifts are 5.2 nm and 10.6 nm, respectively. For a lattice constant of 700 nm, the centre wavelength is 570.70 nm and the blue shift is 15.6 nm, which is the largest shift among these PhCs. To confirm the shift, the spectra of QDs in Fig. 1 were fitted to BiGaussian function (sum of two terms of a Gaussian function) for comparison.

The coincidence of the spectra with the single Gaussian function is not high, which may indicate that PL from QDs does not decay via a single pathway. Therefore, we fitted the spectra from QDs on PhCs to a BiGaussian function (sum of two terms of a Gaussian function), as shown in Fig. 2. It can be seen that all the spectra from QDs on PhCs can be fitted well to BiGaussian functions, except those for PhCs with lattice constants of 900 nm and 750 nm, which can be fitted well to a single Gaussian function. After fitting, the spectra from QDs on PhCs can be divided into two parts, one is a long component at a long wavelength, and the other is a short component at a short wavelength. The long component is denoted as X emission, while the short component is denoted as X\* emission.

The parameters for the spectra from QDs on PhCs fitted to the BiGaussian function depend on the lattice constant, and they are shown in Fig. 3. From Fig. 3a, the centre wavelengths of both the X emission and the X\* emission of QDs on PhCs are shorter than those of the spectra without PhCs. As analysed above, by fitting to a single Gaussian function, the spectra of QDs on PhCs shift to the blue compared with those on the blank. The central wavelengths of both X and X\* vary with PhC lattice constant. The variation range of the centre wavelength (deviation between the maximum and minimum in the wavelength range 577.93–585.69 nm) of X is 7.7 nm, while

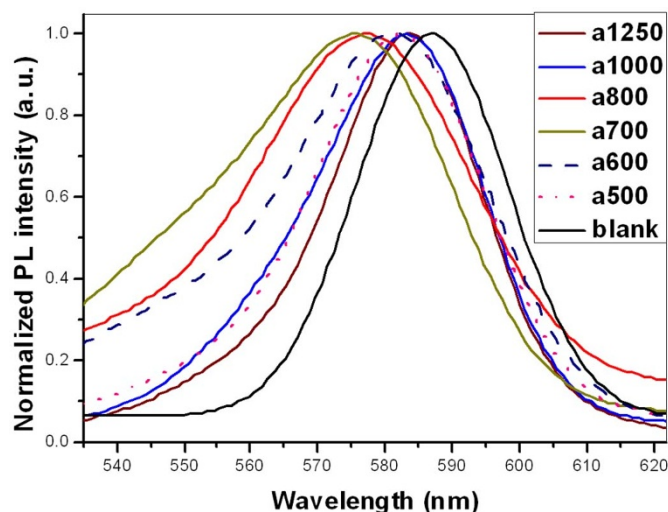


**Figure 1 | The TPF spectra from QDs on PhCs and blank.** Normalized TPF spectra from QDs on PhCs with lattice constants of 1250 nm, 1000 nm, 800 nm, 750 nm, 700 nm and 600 nm, compared with that from QDs on blank SiN; the spectrum from the blank is averaged from four spectra of QDs in different positions of blank SiN without PhCs. The values represent the lattice constants; “blank” means the SiN membrane without PhC.

that (in the range 446.01–578.89 nm) of X\* reaches 32.9 nm. Compared to X\*, the variation of the centre wavelength of X is relatively stable. The largest blue shift of 40.38 nm (deviation between the centre wavelength of the spectra of QDs on PhCs and that on blank) for X\* is for the lattice constant of 800 nm, where the enhancement factor is only around 4. For lattice constants of 1000 nm and 1250 nm, the enhancement factor is larger than 40 and the blue shift of X\* is only around 10.9 nm. The spectral width for X and X\* is shown in Fig. 3b, where the spectral width of X\* is much broader than that of X. The spectral width of X\* is around 19 nm, while that of X is around 11 nm. The spectral widths of X and X\* are similar for lattice constants of 500 nm and 550 nm. Moreover, the overall variation tendency is that the spectral width slightly decreases with increasing lattice constant. The ratio of the X\* and X components is shown in Fig. 3c. The ratio of the X component is larger than 0.5, while that of X\* is less than 0.5 but larger than 0.1. Therefore, the relative efficiencies of X\* are all larger than 10%, and the largest reaches 46.7%. The large ratios of the X component are at lattice constants of 500 nm, 550 nm and 800 nm, with values of 0.88, 0.87 and 0.85, respectively. In contrast, the corresponding ratios of the X\* component at the same lattice constants are small. To some extent, the shorter the centre wavelength of X\*, the smaller the ratio of the component of X\*. From the decay process that can be fitted to a tri-exponential function, the ratio of multi-exciton to exciton emission is about 0.25 (from the result of QDs on SiN membranes). However, in the experiment measuring TPF spectra, the detector is a CCD whose response time is longer than 1 ns; thus the detected TPF spectra do not include multi-exciton emission. From the characterization of TPF spectra, the X component is exciton emission, while the X\* component, thus the large blue shift of the TPF spectra of QDs on PhCs, is attributed to positive trion (charged exciton) emission<sup>3</sup>. Time-resolved PL experiments will demonstrate further that the short X\* component from the BiGaussian fitting is the emission from a trion. The trion state leads to a reduction in PL in nanocrystals on these PhCs. The surface state results in a dim state facilitating the transition to the *off* state and an increase of non-radiative relaxation due to the formation of trion emission<sup>5</sup>. In PhCs with different lattice constants, the local density of states (LDOS) is different, and thus the electric fields corresponding to excitation light

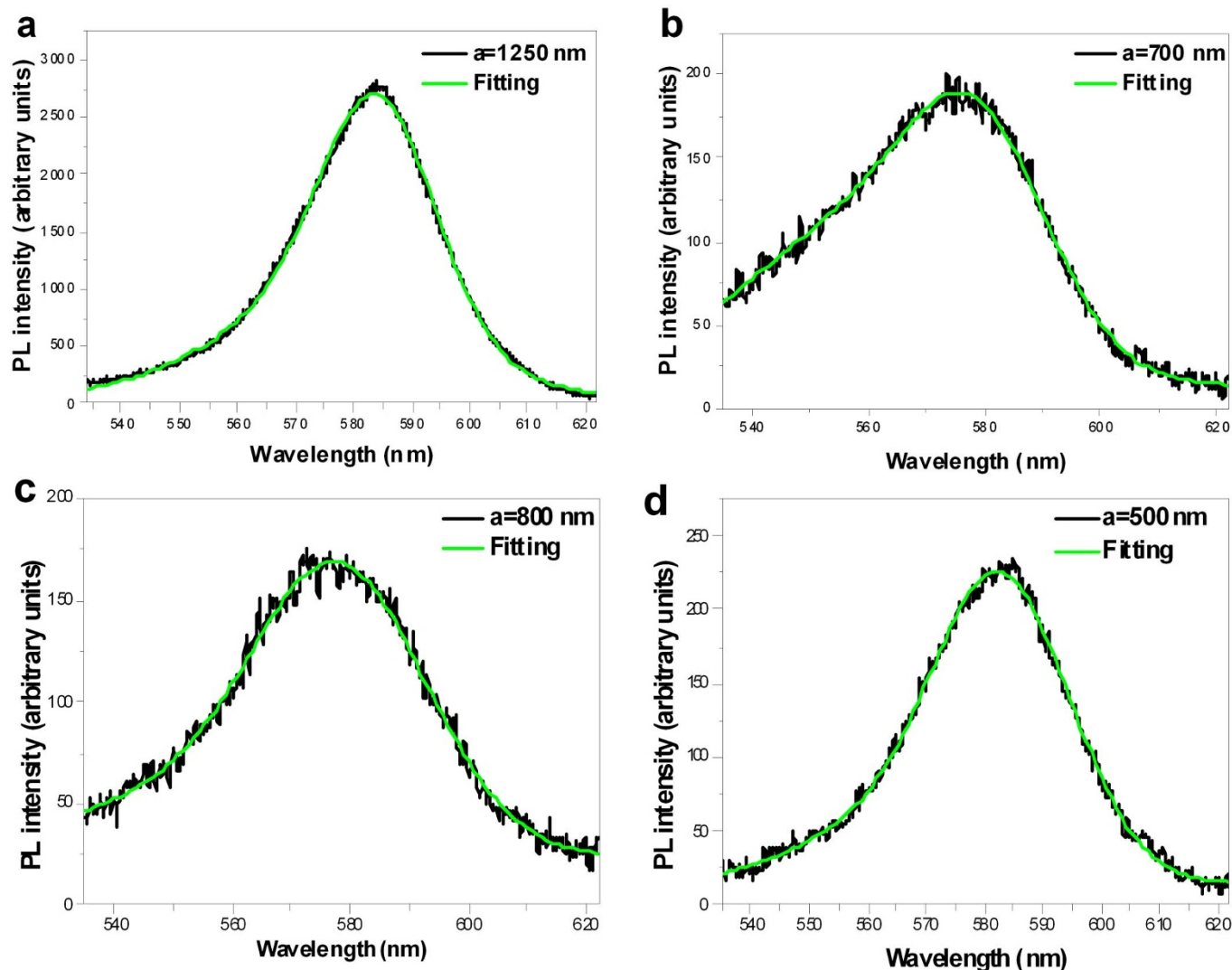


**Figure 2 | Spectra from QDs on PhCs fitted by BiGaussian functions.** The PhC lattice constants are (a) 1250 nm, (b) 700 nm, (c) 800 nm and (d) 500 nm. The spectra are measured at the same excitation intensity. The black lines are the TPF spectra measured from QDs on PhCs, and the green lines are the fitting lines of BiGaussian functions.

and emission light are different. Therefore, the LDOS in PhCs will change the ionization states, and then the emission wavelength of charged exciton (trion) varies with lattice constant, as shown in Fig. 3a. Figure 3c, d shows that the relative efficiency of trion  $X^*$  is larger than 10% and the ratios of the component of trion  $X^*$  to that of exciton  $X$  on these PhCs are larger than 0.1, the largest ratio reaching 0.87 for a lattice constant of 1000 nm. Due to the similar emission level, the trion and the exciton may be explored as a two-photon entangled source. This ratio is much larger than that predicted by the charging model for blinking, where the trion represents the *off* state, while the exciton represents the *on* state in the charging model.

**Mechanism to the asymmetry of TPF spectra.** From Figs. 2 and 3, the intensity of TPF depends on the lattice constants of PhCs, and TPF from QDs on PhCs is highly enhanced compared to that without PhCs. The enhancement mechanism is that excitation light and emission light are resonant with the leaky mode of the PhC slab<sup>14,20</sup>. We correlate the TPF enhancements with the presence of photonic modes near the  $\Gamma$  point for the peak emission wavelength of 585 nm, and note that the pump wavelength of 800 nm is resonant with the leaky mode of the PhC slab. The field enhancement is explained by considering the photonic band

structure of the PhCs shown in Fig. 4. Two points should be mentioned. The first is that the spectral width of the femtosecond laser is not so narrow. As measured, the full width at half maximum reaches about 10 nm. This means that as we use a femtosecond laser with a centre wavelength of 800 nm, the actual pump wavelength ranges from about 795 nm to 805 nm. The second point concerns the irradiation and collection angle of pump light and emission light, respectively. We used an objective lens with a magnification of  $40\times$ . The irradiation and collection angle is about  $-2.3^\circ$  to  $2.3^\circ$ , the  $k$ -vector ranges from 0 to 0.04 ( $\sin(2.3^\circ)$ ), which is shown by the vertical dotted line in the band structure in Fig. 4. For a lattice constant of 1250 nm, the pump wavelength of 800 nm corresponds to the normalized frequency of  $1.5625a/\lambda$ , and is indicated as point A at a leaky mode of the PhC slab in Fig. 4. For a lattice constant of 1000 nm, the pumping wavelength of 800 nm corresponds to the normalized frequency of  $1.25a/\lambda$ , and is indicated by point B at a leaky mode of the PhC slab. Therefore, the electric fields of the pump light in PhCs with lattice constants of 1250 nm and 1000 nm are significantly enhanced and the ratio of trion is large. However, there is also a leaky mode at a normalized frequency of  $1.0625a/\lambda$  ( $a = 850$  nm at pump wavelength of 800 nm), while the ratio of trion for the PhC with lattice constant of 850 nm is smaller. The reason is that, for lattice constants of 1250 nm and 1000 nm, there are also leaky

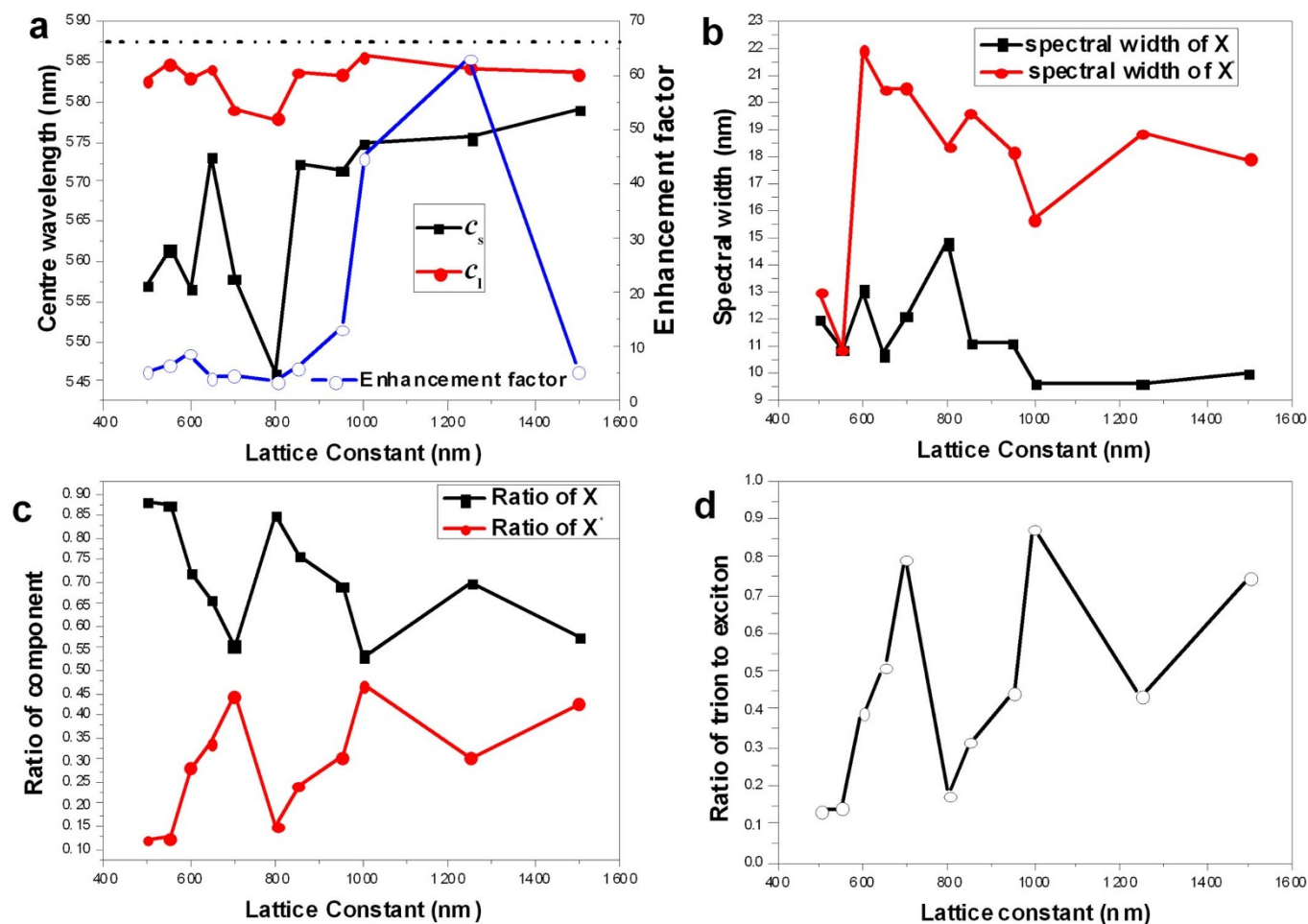


**Figure 3** | The parameters from the spectra fitted by BiGaussian functions for different PhC lattice constants. (a) Centre wavelength of spectra fitted to a BiGaussian function of QDs on PhCs with different lattice constants, where  $c_l$  and  $c_s$  are the centre wavelengths of the long and short components, respectively. Integrated enhancement factor for different lattice constants is shown. Dotted line represents the centre wavelength of spectrum on SiN film without PhCs. (b) Spectral width. (c) Ratio of X and X\* components. These ratios represent the relative emission efficiency of X and X\*. (d) Ratio of X\* to X.

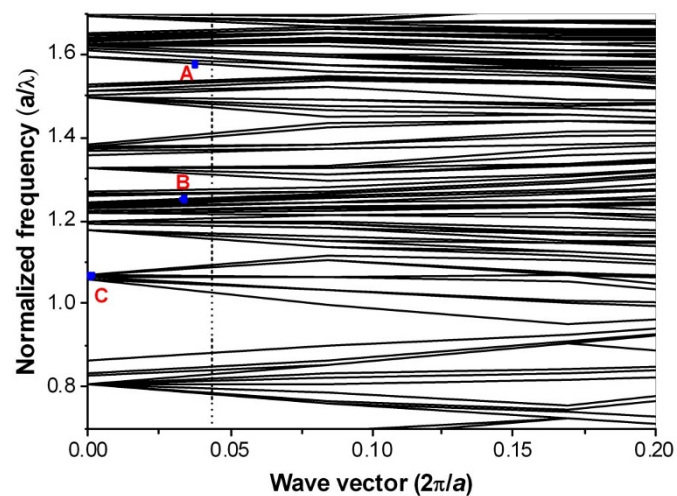


**Figure 4** | Band structure of the PhC. The blue spots A ( $1.5625a/\lambda$ ), B ( $1.25a/\lambda$ ) and C ( $1.0625a/\lambda$ ) correspond to the leaky modes of the PhC slab with respective lattice constants of 1250 nm, 1000 nm and 850 nm at an excitation wavelength of 800 nm.

modes in the band structure overlapping or nearly overlapping with the main emission band around 585 nm, while for the lattice constant of 850 nm, there is no corresponding mode.

To study the enhancement of the spectra of QDs on PhCs, the ratio of the PL intensity of QDs on PhCs to that on blank without PhCs is calculated (See Fig. S3). For different lattice constants ranging from 1500 nm to 500 nm, the peaks of the enhancement factor are located at approximately the same wavelength, which is centred around 555–558 nm with broad spectral width. The enhancement peaks at 555–558 nm in Fig. S3 is attributed to the trion emission. It is difficult to find leaky modes in the band structure that meet the same peak with different lattice constants.

To demonstrate the above analysis, time-resolved PL was measured over a 50 ns time range from the same QDs on SiN membrane by using a streak scope (see methods). The spectra with an excitation power of 300  $\mu$ W at delay of 0 ns integrated in a 950 ps gate (curve F), a delay of 1 ns at a gate of 1 ns (curve M), and a delay of 15 ns at a gate of 4.5 ns (curve S) were recorded and shown, respectively, as black, red and blue lines in Fig. 5a. Curve F contains multi-exciton emission and single exciton, and curve M contains trion emission and single exciton<sup>23</sup>. By fitting the spectra to a Gaussian function, the centre wavelength of curve S (exciton emission) is 594.5 nm with a spectral width of 15.52 nm and the centre wavelength of curve M is 589.30 nm with a spectral width of 17.3 nm. From Fig. 5a, the spectrum of curve M, thus the trion spectrum is shifted to the blue

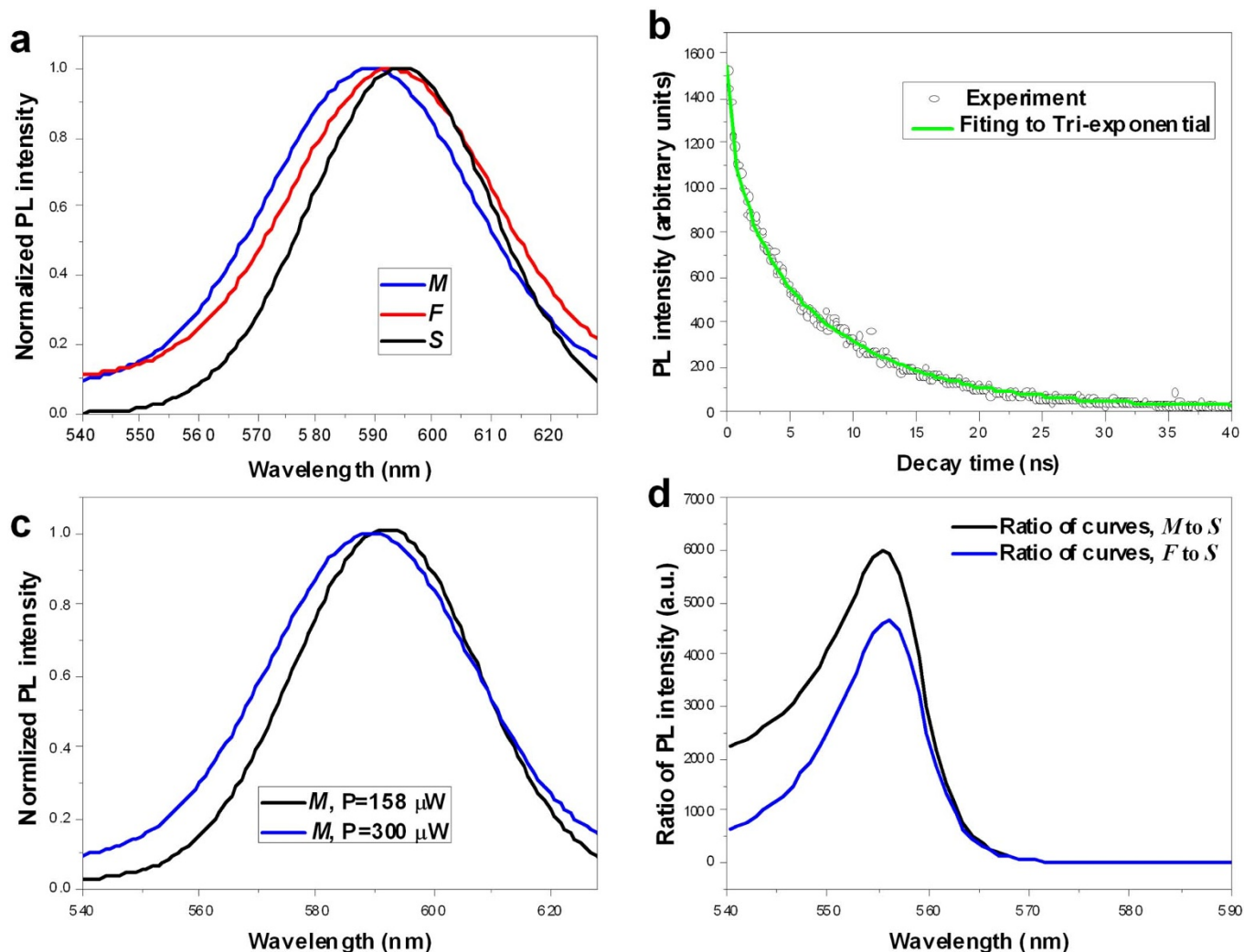


**Figure 5** | TPF spectra and the decay process of QDs on SiN material measured using a streak camera. (a) Time-resolved PL under  $300 \mu\text{W}$  excitation over 50 ns. Curve *F* at delay 0 ns, integrated in 950 ps, curve *M* at delay 1 ns gate 1 ns and curve *S* at delay 15 ns gate 4.5 ns, respectively. (b) Decay process of QDs on SiN membrane, corresponding to the PL in a. (c) Time-resolved spectra at delay 1 ns gate 1 ns (curve *M* in a) at different excitation intensities under 800 nm femtosecond laser excitation. (d) Ratios of curves *F* and *M* to *S*.

compared with that of exciton. The decay process of PL from QDs on SiN membrane is shown in Fig. 5b. The green line is a fitted tri-exponential curve, where obtained lifetimes of 8.91 ns, 1.77 ns and 0.28 ns represent lifetimes of exciton, trion and multi-exciton, respectively. From the fitted amplitude in Fig. 5b, the ratio of trion to exciton reaches 43%, and the relative trion efficiency is 12.8%. This result is in accordance with that obtained from the PL spectra in Fig. 3c. In a previous study<sup>4</sup>, by measuring the PL decay process, a 10–15% quantum yield for trion emission was obtained. Here, by studying both PL decay and PL spectra, we obtain a trion efficiency larger than 10% from CdSe/ZnS QDs on SiN membranes or on SiN PhC slabs, and the largest trion efficiency for QDs on PhCs reaches 46.7%. Moreover, from Fig. 5c, as the excitation intensity increases, the *M*-spectrum, thus the spectrum of the trion emission shifts to the blue. The ratios of the PL intensity of curve *F* and that of *M* to that of *S* are shown in Fig. 5d. The spectral intensities of curve *M* and curve *F* in the short-wavelength region are enhanced significantly compared with those of the exciton, and both ratio peaks are at around 555 nm, which is in accordance with the ratio of PL spectra from QDs in Fig. S3. Fig. S4 shows the time-resolved TPF spectra of QDs on PhCs measured using a streak camera, where the spectrum of curve *M*, thus the trion spectrum is shifted to the blue compared with that of exciton, and the PL intensity of curve *M* (thus the trion spectrum)

in the short wavelength region is much stronger than that of exciton spectrum.

Some previous reports revealed that photo-oxidation by oxygen and water molecules results in a large blue shift for CdSe/ZnS nanocrystals. However, the blue shift is not due to photo-oxidation in our study because the measurement conditions for PhCs and the blank without PhCs are the same. If this blue shift was a result of photo-oxidation, the size of the QD core would reduce, and at the same time, the PL intensity would decrease<sup>24</sup>. In contrast, we observed that the two-photon PL intensity increased with an increase in the blue shift of the spectra.

## Discussion

In conclusion, under two-photon excitation, the QDs absorb two-photon light and emit visible light around 585 nm. Comparison of the spectra of QDs on PhCs with those on blank material indicates that the TPF from QDs on PhCs is significantly enhanced. The electric field for the excitation wavelength is enhanced because the LDOS in the PhCs is enhanced compared with that in blank material. The enhanced electric fields of the excitation light and emission light result in both enhancements of the intensity of TPF and blue shift of the TPF spectrum. In PhCs, excitation intensity is enhanced, and under the relatively strong field of excitation light in PhCs, which



will introduce the DC Stark effect<sup>25</sup>, the charged exciton emission is generated. Moreover, due to the two-photon excitation energy being above the band gap of CdSe, the optical Stark effect<sup>26</sup> may also take effect. Therefore, the blue shift of TPF spectra of QDs on PhCs is mainly attributed to charged exciton (trion) emission. It has been proved that for emitters in PhC membranes, the lifetime of emission in the photonic band region is similar to or only decreases to approximately 80% of that of the blank material without PhCs<sup>21</sup>. PhC membranes will not decrease much the emission lifetime of QDs directly, but the PhCs enhance the excitation intensity, the trion and multi-exciton emission efficiency. Therefore, the enhancement of trion emission is mainly due to the change in QD microscopic structure and decay path of PL. The time-resolved experiments demonstrate further that the blue shift of spectra of QDs on PhCs mainly arises from charged exciton (trion) emission. On some PhCs, the ratio of trion to exciton reaches 0.87, which means that the charging model is not suitable here, and the enhancement is due to the trion emission coupling to the leaky mode of the PhC slab. Therefore, the model of the mechanism for blinking on PhCs should combine the charging model with the enhancement effect of PhCs. This means that PhCs enhance the trion PL intensity and also modify the spectrum. This process is believed to be caused by the enhancement of the electric field introduced by the charge separation between the charge in the nanocrystal core and that of the surface states. PhCs enhance the Auger-assisted trapping efficiency of electrons/holes to surface states, and then enhance the efficiency of charge separation and generation of DC electric field that modifies the trion spectrum. Therefore, PhCs enhance the DC Stark effect created by charge separation, and the different DC Stark effect in PhCs results in different trion emission intensity and emission wavelength.

TPF from CdSe/ZnS nanocrystals on PhCs undergoes a blue shift when compared with that without PhCs. The maximum blue shift of the TPF spectra is 40 nm. The largest ratio of the trion to exciton components reaches 87%, and the high efficiency of the trion may make it possible to explore excitons and trions as a two-photon entangled source. The blue shift and enhancement of the TPF PL intensity are due to coupling of pump light and TPF emission to the leaky modes of the PhC slab. The asymmetry of the PL spectra from PhCs with different lattice constant is due to combined effect of enhancement from PhCs and trion emission from colloidal QDs. The strong electric field of the pump light and TPF in the PhCs results in an enhancement of the Auger-assisted trapping efficiency of electrons/holes to surface states, and the efficiency of charge separation and generation of a DC electric field, and then positive trion emission takes place. This phenomenon indicates that trion emission and blinking of colloidal nanocrystals depend on the environment; combining the charging model and PhC enhancement effect can explain the blinking phenomenon of QDs on PhCs. Therefore, we deduced that a model for QDs blinking should include Auger process and Auger-assisted surface recombination.

## Methods

In the measurement of TPF from colloidal QDs, a femtosecond laser with a pulse width of around 80 fs, repetition frequency of 80 MHz and wavelength of 800 nm was focused onto the sample with a 40× objective lens at room temperature. The TPF was collected by the same objective lens in the vertical direction. The average excitation power before the objective lens was 56 mW. The emission light was collected into a spectrometer equipped with a silicon CCD (Hamamatsu).

Time-resolved PL was measured over a 50 ns time range from the same QDs on SiN membrane by using a streak scope (Hamamatsu). A femtosecond laser with a pulse width of 120 fs, repetition frequency of 1 kHz and wavelength of 800 nm is focused by a 20× objective lens. The sample was colloidal CdSe QDs on a SiN film. The average excitation power before the objective lens was 300 μW.

Two-dimensional photonic crystals on SiN membrane were fabricated by electron beam lithography and reactive ion etching<sup>22</sup>. The thickness of SiN film was 160 nm SiN film, which was deposited on a silicon substrate using plasma-enhanced chemical vapor deposition. The refractive index of the SiN material was 1.99. The lattice constants ranged from 400 nm to 1500 nm. After dry etching, the silicon under SiN membrane was removed by HNA (HF:Nitric:Acetic) mixture to form a free-standing structure. The colloidal quantum dots were casted onto the surface of SiN photonic crystals.

Fitting of the spectra was done using Origin 8.0 software. To investigate the physical mechanism behind the asymmetry of the PL spectrum, the measured spectrum was fitted to a BiGaussian function

$$y = y_0 + A_l \exp\left(-\frac{(x-c_l)^2}{2\omega_l^2}\right) + A_s \exp\left(-\frac{(x-c_s)^2}{2\omega_s^2}\right),$$

where  $A_l$  and  $A_s$  are the amplitudes of the two Gaussian components,  $\omega_l$  and  $\omega_s$  are the spectral widths,  $c_l$  and  $c_s$  are the centre wavelengths, and  $y_0$  is the relative amplitude.

- Efros, A. L. & Rosen, M. Random telegraph signal in the photoluminescence intensity of a single quantum dot. *Phys. Rev. Lett.* **78**, 1110–1113 (1997).
- Galland, G. *et al.* Two types of luminescence blinking revealed by spectroelectrochemistry of single quantum dots. *Nature* **479**, 203–208 (2011).
- Saba, M. *et al.* Light-induced charged and trap states in colloidal nanocrystals detected by variable pulse rate photoluminescence spectroscopy. *ACS Nano* **7**, 229 (2013).
- Jha, P. P. & Guyot-Sionnest, P. Trion decay in colloidal quantum dots. *ACS Nano* **3**, 1011–1015 (2009).
- Gómez, D. E., van Embden, J., Mulvaney, P., Fernée, M. J. & Rubinsztein-Dunlop, H. Exciton–trion transitions in single CdSe–CdS core–shell nanocrystals. *ACS Nano* **3**, 2281–2287 (2009).
- Lodahl, P. *et al.* Controlling the dynamics of spontaneous emission from quantum dots by photonic crystals. *Nature* **430**, 654 (2004).
- Fujita, M., Takahashi, S., Tanaka, Y., Asano, T. & Noda, S. Simultaneous inhibition and redistribution of spontaneous light emission in photonic crystals. *Science* **308**, 1296 (2004).
- Wijnhoven, J. E. G. J. & Vos, W. L. Preparation of photonic crystals made of air spheres in titania. *Science* **281**, 802 (1998).
- Yamaguchi, M., Fujita, M., Asano, T., Nakanishi, J. & Noda, S. Investigation of spontaneous emission from quantum dots embedded in two-dimensional photonic-crystal slab. *Electron. Lett.* **41**, 1402 (2005).
- Hennessy, K. *et al.* Quantum nature of a strongly coupled single quantum dot-cavity system. *Nature* **445**, 896 (2007).
- Badolato, A. *et al.* Deterministic coupling of single quantum dots to single nanocavity modes. *Science* **308**, 1158 (2005).
- Ganesh, N. *et al.* Enhanced fluorescence emission from quantum dots on a photonic crystal surface. *Nat. Nanotechnol.* **2**, 515 (2007).
- Ren, F.-F. *et al.* Strong vertical light output from thin silicon rich oxide/SiO<sub>2</sub> multilayers via in-plane modulation of photonic crystal patterns. *Appl. Phys. Lett.* **93**, 091901 (2007).
- Fan, S., Villeneuve, P. R., Joannopoulos, J. D. & Schubert, E. F. High extraction efficiency of spontaneous emission from slabs of photonic crystals. *Phys. Rev. Lett.* **78**, 3294 (1997).
- Boroditsky, M. *et al.* Light extraction from optically pumped light-emitting diode by thin-slab photonic crystals. *Appl. Phys. Lett.* **75**, 1036 (1999).
- Erchak, A. A. *et al.* Enhanced coupling to vertical radiation using a two-dimensional photonic crystal in a semiconductor light-emitting diode. *Appl. Phys. Lett.* **78**, 563 (2001).
- Ryu, H. Y., Lee, Y. H., Sellin, R. L. & Bimberg, D. Over 30-fold enhancement of light extraction from free-standing photonic crystal slabs with InGaAs quantum dots at low temperature. *Appl. Phys. Lett.* **79**, 3573 (2001).
- Kim, J. Y. *et al.* Enhanced light extraction from GaN-based green light-emitting diode with photonic crystal. *Appl. Phys. Lett.* **91**, 181109 (2007).
- Kim, S. H. *et al.* Fabrication of photonic crystal structures on light emitting diodes by nanoimprint lithograph. *Nanotechnology* **18**, 055306 (2007).
- Inoue, S. I. & Yokoyama, S. Enhancement of two-photon excited fluorescence in two-dimensional nonlinear optical polymer photonic crystal waveguides. *Appl. Phys. Lett.* **93**, 111110 (2008).
- Fujita, M., Takahashi, S., Tanaka, Y., Asano, T. & Noda, S. Stimulated inhibition and redistribution of spontaneous light emission in photonic crystals. *Science* **308**, 1296 (2005).
- Xu, X. S., Yamada, T., Ueda, R. & Otomo, A. Two-photon excited fluorescence from CdSe quantum dots on SiN photonic crystals. *Appl. Phys. Lett.* **95**, 221113 (2009).
- Marceddu, M. *et al.* Charged excitons, Auger recombination and optical gain in CdSe/CdS nanocrystals. *Nanotechnology* **23**, 015301 (2012).
- Wang, X., Zhang, J., Nazzari, A. & Xiao, M. Photo-oxidation-enhanced coupling in densely packed CdSe quantum-dot films. *Appl. Phys. Lett.* **83**, 162 (2003).
- Klimov, V. I. & McBranch, D. W. Auger-process-induced charge separation in semiconductor nanocrystals. *Phys. Rev. B* **55**, 13173 (1997).
- Schaller, R. D., Agranovich, V. M. & Klimov, V. I. High-efficiency carrier multiplication through direct photogeneration of multi-excitons via virtual single-exciton states. *Nature Phys.* **1**, 189–194 (2005).

## Acknowledgments

We acknowledge financial support from the National Basic Research Program under Grant No 2013CB632105, the National Natural Science Foundation of China under Grant Nos 91121019, 61275045 and 61021003.



## Additional information

Supplementary information accompanies this paper at <http://www.nature.com/scientificreports>

**Competing financial interests:** The author declares no competing financial interests.

**How to cite this article:** Xu, X.S. Enhanced trion emission from colloidal quantum dots with photonic crystals by two-photon excitation. *Sci. Rep.* 3, 3228; DOI:10.1038/srep03228 (2013).



This work is licensed under a Creative Commons Attribution-NonCommercial-NoDerivs 3.0 Unported license. To view a copy of this license, visit <http://creativecommons.org/licenses/by-nc-nd/3.0>